Signatures of Current Loop Coalescence in Solar Flares

J.Sakai[1], T.Tajima[2], H.Nakajima[3],
T.Kosugi[3], F.Brunel[4], E.Zaidman[2]

1 Faculty of Engineering, Toyama University, Toyama 930 JAPAN

2 Department of Physics, University of Texas, Austin, Texas U.S.A.

3 Nobeyama Solar Radio Observatory, University of Tokyo, JAPAN

4 National Research Council, Ottawa, CANADA

Abstract

The nonlinear coalescence instability of current carrying solar loops can explain many of the characteristics of the solar flares such as their impulsive nature, heating and high energy particle acceleration, amplitude oscillations of electromagnetic emission as well as the characteristics of 2-D microwave images obtained during a solar flare. The physical characteristics of the explosive coalescence of currents are presented in detail through computer simulation and theory.

Canonical characteristics of the explosive coalescence are:

⑴ a large amount of impulsive increase of kinetic energies of electrons and ions,

⑵ simultaneous heating and acceleration of electrons and ions in high and low energy spectra,

⑶ ensuing quasi-periodic amplitude oscillations in fields and particle quantities,

⑷ the double peak (or triple peak) structure in these profiles, and

⑸ characteristic break in energy spectra of electrons and ions.

A single pair of currents as well as multiple currents may participate in the coalescence process, yielding varieties of phenomena. These physical properties seem to underlie in some of impulsive solar flares.

In particular, double sub-peak structures in the quasi-periodic oscillations found in the time profiles of two solar flares on June 7, 1980 and November 26, 1982 are well explained in terms of the coalescence instability of two current loops. This interpretation is supported by the observations of two microwave sources and their interaction for the November 26, 1982 flare.

Some more details as well as a generalization of the present model to solar flares with the coalescence as an elementary process in the flare phenomenon are presented.

1. Introduction

The solar flare phenomenon is a manifestation of an explosive release process of energy stored in the lower corona, involving the plasma heating up to 5×10^7 K, the acceleration of charged particles up to the order of the rest mass energy of electrons and ions, as well as the production of electromagnetic radiation from the radio band to γ-ray wavelengths. (for a previous summary of solar flares, see

Svestka, 1976; Sturrock, ed., 1980; Priest, 1982).

After launching of the Solar Maximum Mission (SMM) and Hinotori satellites, it becomes clear from the observations of hard X-rays and γ-rays that the electrons with energies up to MeV as well as ions with energies up to GeV can be simultaneously accelerated within a second during the impulsive phase of a solar flare. In a particular flare (03:12UT of June 7, 1980) the γ-rays showed a quasi-periodic amplitude oscillation which closely correlated with the quasi-periodicity in both microwave bursts and hard X-ray bursts.

Direct observations in soft X-rays (Howard and Svestka, 1977) showed that in the active regions there exist multiple coronal loops which might carry plasma currents. The interconnecting coronal loop might be a quite important physical process for energy release in the solar corona.

Recently, the observations of the interacting coronal loops which lead to solar flares have increased in various kinds of observations from H_α (Kurokawa et al., 1985), radio (Nakajima et al., 1984) as well as hard Y-ray (Machado, 1985).

In order to explain the rapid quasi-periodic particle acceleration of both electrons and ions observed in the June 7, 1980 flare, Tajima et al., (1982, 1985) showed that the most likely mechanism for the impulsive energy release in solar flares is the current loop coalescence instability (Finn and Kaw, 1977, Pritchett and Wu, 1979).

It has been shown that by simulation and theory (Tajima and Sakai, 1985) that dring the coalescence of two current loops, the magnetic energy stored by the plasma current can be explosively transformed to the plasma heating as well as the production of high energy particles within a transit Alfvén time across the current loop (which is about $1 \sim 10$ seconds for appropriate radius of the loop) through the magnetic reconnection process. Furthermore, the energy release can be achieved with quasi-periodic fashion whose periodicity depends on plasma parameters such as plasma beta ratio (β), the ratio B_P/B_T between the magnetic field, B_P produced by the plasma current and B_T the pntential magnetic field, as well as the colliding velocity of two current loops that is determined mostly from the initial total plasma loop current.

The plasma can be heated up to 60 times of the initial temperature and the electrons and ions can be accelerated simultaneously by the transverse electrostatic field which can be produced during the explosive coalescence process.

The present paper is to show results obtained from current loop coalescence plasma dynamics with applications to solar flares. The current loop coalescence itself is similar with Gold and Hoyle model (1960) and emerging flux model (Hayverts et al., 1977) in its morphological spirit of the model. However, the details are quite different from each other. In particular, Tajima and Sakai (1985) presented the physical basis of such a morphological model, i.e., the physics of magnetic reconnection process, as well as particle acceleration mechanism. We found basically two types of magnetic reconnection, namely, slow and explosive processes: the reconnected magnetic flux $\varDelta \psi$ is proportional to t^m ($m > 1$) in the slow reconnection process and $\varDelta \psi$ is proportional to $(t_0 - t)^{-m}$ ($m > 0$), in the explosive process. We also found in the ensuing stage the quasi-periodic reconnection with quasi-periodic acceleration during the coalescence of current loops.

2. **Physical Characteristics of Current Loop Coalescence**

In the problem of solar flares, the reconnection of field-lines is believed to take place due to finite resistivity. The paper based on a boundary layer analysis by Furth, Killeen, and Rosenbluth found an instability (the tearing instability) which grows at a growth rate $\gamma = C \tau_r^{-3/5} \tau_A^{-2/5} \propto \eta^{3/5}$.

Sweet and Parker, on the other hand, obtained a steady-state solution which has a narrow x-point angle; the time scale τ_{SP} of reconnection is characterized by $\tau_{SP}^{-1} = \sqrt{\eta} \, (n_i/n_e)^{1/2} (V_A/L)^{1/2} \, x_0^{-1} \propto \sqrt{\eta}$, where $2L$ is the length of the impinged plasma, and n_i and n_e are the densities inside and outside of the singular layer. Petschek similarly obtained a steady-state solution which has a large x-point angle; the reconnection time scale τ_P is independent of resistivity, $\tau_P^{-1} \propto \eta^0$. The time scale of reconnection due to the mechanism of the Sweet-Parker process is characterized by $\varepsilon^{-\frac{1}{2}}$ ($\varepsilon = \tau_A/\tau_r$), while that of Petschek is by ε^0. It may be said that the paper by Furth et al. is appropriate for situations of spontaneously growing tearing modes, while the papers by Sweet et al. are for problems of driven reconnection, although the distinction is yet to be clarified in more precise scientific terms.

Since the paper by Furth et al. was published, a considerable amount of literatures have been written which further investigate the nonlinear processes of the tearing instability. A paper by Rutherford discussed nonlinear secular growth of a single tearing mode, while a paper by Drake and Lee found the collisionless equivalent to the Rutherford regime. The Rutherford time scale τ_R^{-1} is characterized by $\tau_R^{-1} \cong C \eta \Delta' (B_y \, \psi)^{1/2}$, where C is a constant less than unity, B_y is the shear field, and ψ the reconnecting flux. Carreras, Rosenbluth, Diamond et al. discussed.nonlinear stages of many tearing modes with different helicities (i.e., on different rational surfaces), emphasizing mode couplings. With more than one helicity, the coupling is inherently three dimensional.

It has been recognized that the processes of magnetic reconnection are quite different depending upon whether reconnection is driven or spontaneous. For the spontaneous cases, as we briefly reviewed in the above paragraph, the current sheet becomes unstable against the tearing instability evolving from the unstable magnetic configuration. It is customary to argue that the Rutherford regime follows the linear stage and then the highly nonlinear mode coupling stages come into play. There are natural disturbances such as solar flares and geomagnetic storms, in which some of the observed time scales of the entire process of explosive phenomena are as small as the Alfvén time. The scenario for reconnection based on spontaneous tearing has to confront the observed rapid reconnection psocesses, although the nonlinear stages of spontaneous reconnection can be quite rapid, as reviewed in the preceding paragraph. In this case, one has to maintain the unstable configuration in equilibrium long enough to reach the disruptive stage. On the other hand, driven reconnection is much faster and therefore quickly enters the nonlinear stage. This is one of the reasons why the driven reconnection has been studied by many authors.

In order to rapidly convert magnetic energy into kinetic one by a substantial amount, it seems necessary that the bulk of magnetic energy has to participate in the conversion process: the resistive heating at the x-point alone is to meager. This is because the available magnetic energy at the x-point is small by itself. On the other hand, the ideal MHD instabilities such as the kink instability and the coalescence instability are the processes that involve the bulk current

redistribution in a matter of the Alfvén time scale.

In the present paper we pick the coalescence instability as the primary instability to investigate its nonlinear consequences. we do so because (1) although it is an ideal MHD instability for drive in the linear sense, it would not nonlinearly evolve if there is no resistive (non-ideal MHD) effcect; (2) therefore, it can involve a large amount of conversion of magnetic to kinetic energies in a short time; (3) it is essentially a two-dimensional instability, thus more amenable to thorough analysis of the fundamental processes of the instability. It is interesting to observe that with this two-dimensionality restriction we still find an explosive process as we shall see. The coalescence instability starts from the Faddeev equilibrium, which is characterized by the current localization parameter ϵ_c : The equilibrium toroidal current (in the zdirection) is given as $J_z = B_0 \kappa k(1 - \epsilon_c^2)$ (cosh kh + ϵ_c cos kx) . The parameter ϵ_c varies from 0 to 1 with small ϵ_c corresponding to a weak localization and ϵ_c close to unity corresponding to a peaked localization; in the limit of $\epsilon_c \to 1$ the current distribution becomes delta function-like. The rate of reconnection was that of Sweet-Parker for small ϵ_c, while the reconnection rate experiences two phases for larger ϵ_c (but smaller than 0.8). This emergence of two phases is similar to the case of the driven reconnection. The intensity of coalescence and the rate of subsequent reconnection are controlled by just one parameter, the current localization (ϵ_c). In this problem there is no ambiguity as to the nature of the driver in contrast to the reconngection driven by external boundary conditions. For the case with $\epsilon_c = 0.7$, the second phase showed the reconnected flux increasing as t^α with $1 < \alpha < 2$. (Brunel-Tajima scaling) This indicates that the more the current localizes, the faster the reconnection becomes.

As seen in the next section, for the case with $\epsilon_c = 0.85$ we found more rapid reconnection called explosive reconnection, in which the reconnected flux increases as $(t_0 - t)^{-4/3}$. (Tajima-Sakai scaling)

2.1 Summary of Simulation Results

We combine both a MHD model and a kinetic model of simulation. The results from these two different models are consistent in basic points, but are complementary in many detailed aspects. The kinetic simulation model we adopt here is the electromagnetic particle code with $2\frac{1}{2}$ dimensions.

The MHD simulation model we use is the MHD particle code with $2\frac{1}{2}$ dimensions. The MHD particle code is robust in applications to problems even with strong turbulence, flows, convections, and density depression. This is helpful because the present problem involves fast (explosive) reconnection, strong density depression and compression, and strong flows.

Results from the electromagnetic particle model are now discussed. Figure 1 displays the typical time history of various field and particle quantities observed in our simulation in which after the initial transient (up to $t = 4 \, \Omega_i^{-1}$ in the code unit to be explained in the following section) the phase of coalescence of two magnetic islands commences. It is seen in Figs. 1 (a) $-$ (c) that around $t = 27$ the magnetic and electrostatic field energies shoot up explosively as well as the ion temperature in the direction of coalescence (the x-direction). The unit of computational time is omitted hereafter whenever it is unambiguous. It is also seen in Figs. 1 (a)

—(c) that (1) after the explosive increase of the field energies and temperature this overshooting results in synchronous amplitude oscillations of all these quantities with the period being approximately the compressional Alfvén period; and (2) superimposed on these overall amplitude oscillations is a distinct double-peak structure in the electrostatic field energy and the ion temperature. Although we are interested in analyzing the entire episodo of the run including the initial phase and the post-explosive phase, we focus particularly on the explosive phase of the coalescence. We replot Figs· 1 (a) —(c) into Figs. 1 (d) —(f) to find the way in which these quantities increase toward the catastrophic point. We find from Figs. 1(d) —(f) that (1) the magnetic
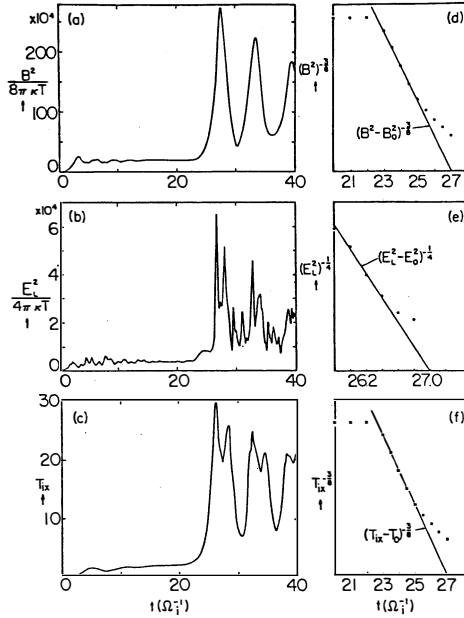

Fig. 1. Explosive increase of field energies and temperature during the coalescence of two magnetic islands: EM particle simulation results. For the case $\Omega_{et} = 0.2$. Other parameters are given in Sec. II. Toward the same explosion time $t = t_o = 27(\Omega_i^{-1})$, the magnetic energy B^2 (a), electrostatic energy E_L^2 (b), and the ion temperature in the x-direction T_{ix} (c) diverge as $(t_o - t)^{-8/3}$, $(t_o - t)^{-4}$, an d $(t_o - t)^{-8/3}$, as shown in (d), (e), and (f), respectively. [We took $B_o^2 \sim 1.6 \times 10^5$, $E_{Lo}^2 \sim 7.5 \times 10^3$, and $T_{ixo} \sim 0.85$ for the pre-explosive phase values; see Figs. 1(a)·(c)].

energy explodes as $(t_0 - t)^{-8/3}$; (2) the electrostatic energy explodes as $(t_0 - t)^{-4}$; and (3) the ion temperature in the coalescing direction explodes as $(t_0 - t)^{-8/3}$ until saturation due to overshooting sets in, where t_0 is the explosion time measured here to be $t_0 \sim 27 (\Omega_i^{-1})$ in this run. Figure 2 presents the time history of various field quantities and temperatures in the course of the early formation and the coalescence with the toroidal field being such that $eB_z/ m_e c = \Omega_{et} = 0.2 \, \omega_{Pe}$. In Fig. 2(a) both the magnetic field energy and the ion temprerature in the direction of coalescence (x) show that after the early ($t \leq 3 \, \Omega_i^{-1}$) rise which corresponds to the magnetic islands formation by tearing a long relatively dormant period ($t = 3 - 22$) sets in, followed by a stage ($t = 22 - 27$) rapid and huge increase in these quantities. It is also evident that after the rapid increase ($t \geq 27$) salient amplitude oscillations ensue due to ovgershooting.
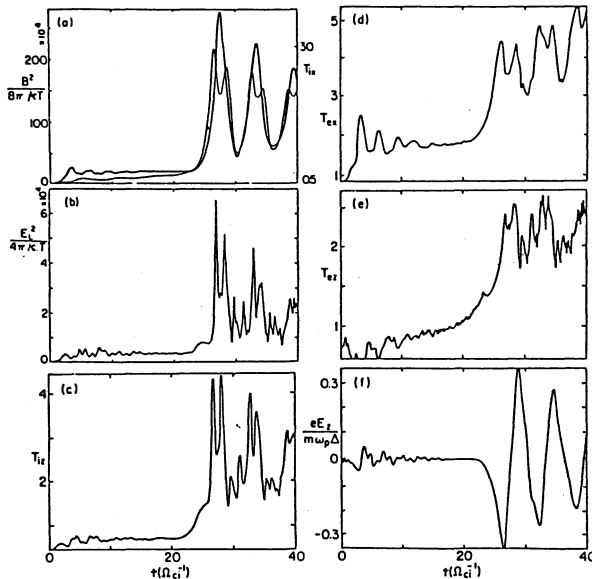
Fig. 2. Temporal profiles of particle and field quantities for the coalescence process obtained from the EM particle simulation. $\Omega^{et} = 0.2$. (a) The thick line represents the magnetic energy, the thin one the ion temperature in the x-direction. (T_{ix} at $t = 0$ was 0.5). (b) Electrostatic field energy in time. (c) Ion temperature in the z-direction. (d) Electron temperature in the x-direction. (e) Electron temperature in the z-direction (f) Inductive electric field (E_z) in time.

It is to be remarked that all the other quantities shown in Fig. 2 (a) $-$(e) closely follow the pattern of Fig. 2 (a) with their characteristic events simultaneously occurring. It is also noted that the amplitude oscillations of the temperatures (T_{ix} and T_z as well as T_{ex} and T_{ez}) and the electrostatic field energy have a structure of marked double peaks. The valley of the double $-$peak structure coincides with the peak of the magnetic field energy amplitude. As mentioned in Sec. 1, it is important to notice that the rapidness of the increase of each quantity differs and and that each quantity explosively increases characterized by a certain definite, but different, index of explosion (i. e., the exponent to the time measured backward from the point of explosion time) until the saturation stage sets in. The stop of rise (t $\sim$3) of each quantity in Fig. 2(a) $-$ (e) corresponds to the completion of islands formation. The following quiescent period ($3 < t < 20$) corresponds to the stage where the formed islands slowly attract each other. The rapid explosive rise (t $\geqq$ 20) marks the commencement of the explosive coalescence. The following stage of amamplitude oscillations correspond to the "breathing" (or pulsations) of coalesced islands (compressional Alfvén oscillations). The induced electric field E_z explosively increases when there is rapid flux reconnection during the explosive coalescence and then oscillates as the magnetic flux in the coalesced island is compressed and decompressed.

Some of the above findings can be given by a qualitative explanation. Since we shall discuss the explosive phase in greater detalil later, we try to pay attention to the amplitude oscillation phase in particular here. Once two current blobs coalesce, they are bound by common magnetic flux. The larger coalesced island continues to vibrate. Within the coalesced island the colliding

two plasma blobs cause turbulent flows which dissipate their energy quickly into heat, thereby reducing the amplitude oscillations of temperatures and field. As a result as we shall see, the momentum distribution of plasma electrons and ions exhibit an intense bulk heating and acceleration of the tail. The heating in the poloidal direction (x) is due to adiabatic compression and decompression of the coalesced current blobs. The eventual bulk heating is a result of turbulent dissipation of counterstreaming instabilities. The heating in the toroidal direction is due to heating/acceleration by the inductive toroidal electric field which is several times the classical Dreicer field and the v_P xB acceleration. The double peak in the time development of the temperatures occur just before $(t=t_1 \sim 27)$ and after $(t=t_3 \sim 29)$ the maxima of magnetic field $(t= t_2 \sim 28)$. In Fig. 3 schematic sequential pictures of plasma dynamical behavior during coales-
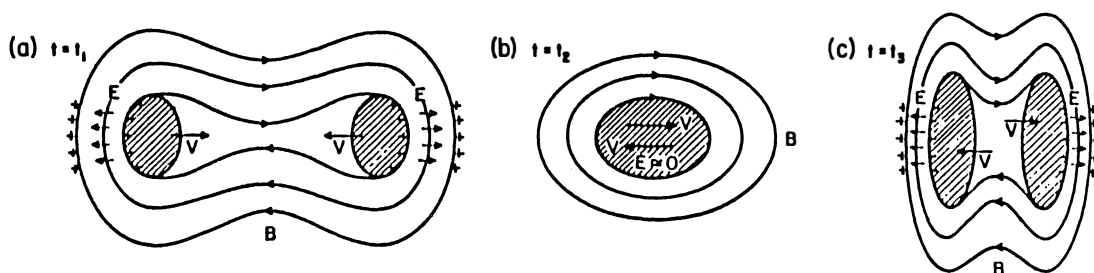

Fig. 3. Schematic sequence of snapshots of the plasma and electric and magnetic fields during the coalescence process.

cence are shown. At $t=t_1$ the magnetic (JxB) acceleration of ions becomes maximum so that the magnetic flux the behind the colliding plasma blobs as well as the plasma blobs are themselves strongly compressed. This plasma compression causes the first temperature peak at $t=t_1$. After this maximum acceleration phase ions aguire substantial velocities along the direction of collision so that they detach from the magnetic flux against which ions have bceen compressed. This result in an expansion phase $(t=t_2)$ of ions, and hence in an adiabatic cooling of the plasma as the magnetic fields obtain maximum values. TIhe process reverses after the maximum of the magnetic fields at $t=t_3 \sim 29 \; \Omega_i^{-1}$, which gives rise to the second peak of the temperature.

The high energy tail particle acceleration of ions and electrons may be qualitatively discussed here. The tail formation is probably due to a combination of localized electrostatic field acceleration across the poloidal magnetic field aund magnetic acceleration of the poloidal to toroidal directions.

Electrons are magnetized and are carried away with the accelerating magnetic flux, while bulk ions are accelerated by the JxB force. On the other hand, the high energy ions are produced and dragged by the charge separation created near the compressed flux. The difference of motions between ions and electrons around $t=t_1$ causes a strong localized shock-like electrostatic field, E_x, which propagates with a phase velocity of the structure $v_P = v_x$. This v_P xB acceleration causes the formation of high energy particle in the toroidal direction. By this acceleration process, ions and electrons are accelerated to relativistic energies in opposite directions along the

toroidal magnetic field.

Next we present the simulation results of the case of multiple coalescence process (Fig. 4). A number of islands are induced as the crowbar current is turned on. An interesting phenomenon
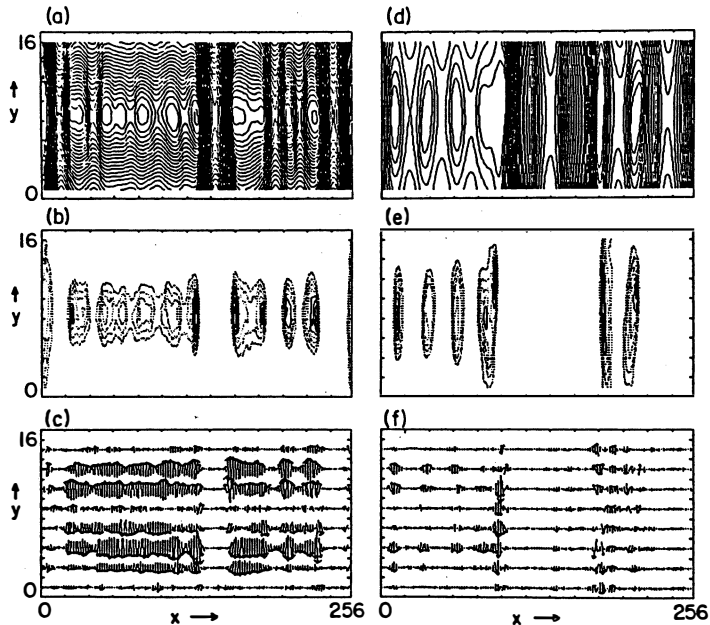

Fig. 4. Multi-loop coalescence; (a)(d); magnetic field line, (b)(e); density
(c)(f); electrostatic field.
(a)(b)(c) correspond to the same time,
and (d)(e)(f) follow.

here is that these islands begin to coalesce one by one to form slightly larger ones. In turn, these larger islands coalesce further into still larger islands. Finally, we are left with only two (big) islands that more resembles two sheets of plasma. Eventually these two islands also coalesce into into but one. In this multiple coalescence process, the early stage presents many less regular or spiky time profiles of fields and particle quantities. As time goes on, larger and more organized time profiles of these quantities come to dominate. Eventually, large scale oscillations are observed in Fig. 5, which are set off after the final two islands coalesce into one. This is, therefore, a similar procerss to the previous two islands coalescence process. In this particular choice of parameters heating and acceleration of particles are more intense than the previous case. Corresponding energy distributions (spectrum) show a longer and more populous tail, indicating a harder spectrum. However, the basic feature of two (for perpendicular) and three (for the z-directional distribution) distinct distribution regimes is still unchanged, implying the same heating/acc acceleration mechanism at work. When we inspect the electron z-direction distribution, the highest energy of the tail oscillates as the overall coalesced island vibrates. On the other hand, the maximum ion energy of the tail in the z-direction, although also oscillating., is less sensitive to the island vibrbation.

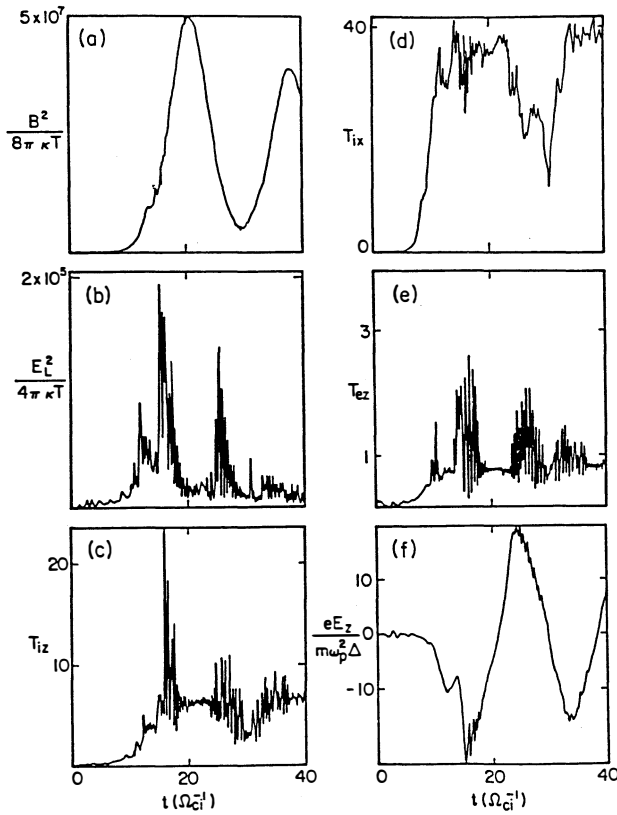Results from the magnetohydrodynamic particle models are presented hence. Fig. 6 shows

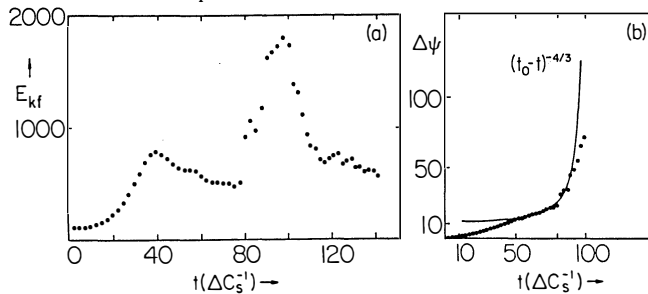Fig. 5. Time hisroty of physical quantities in the case of multi-loop coalescence.

Fig. 6. Temporal profiles of the fluid energy (a) and the reconnected flux (b) for $\epsilon_c = 0.85$ obtained from the MHD particle simulation. A solid line in (b) is a theoretical curve discussed in Sec. III.

kinetic energy and the reconnected flux upon coalescence as a function of time for the case with $\epsilon_c = 0.85$. A theoretical curve $(t_0 - t)^{-4/3}$ is superimposed on the simulation result. During the phase of the rapid increase of reconnected flux ($t = 50 - 90$ Δ c_s^{-1}) the simulation result matches reasonably with the theoretical curve. Beyond $t = 90$ Δ c_s^{-1} the increase begins to be mitigated due to a saturation effect (the flux depletion).

Figre 7 displays the case with $\epsilon_c = 0.7$. The reconnected flux increases rapidly with $\Delta \psi \propto t^m$ ($m = 1.9$). It is, however, less rapid than the case with $\epsilon_c = 0.85$. The released energy is
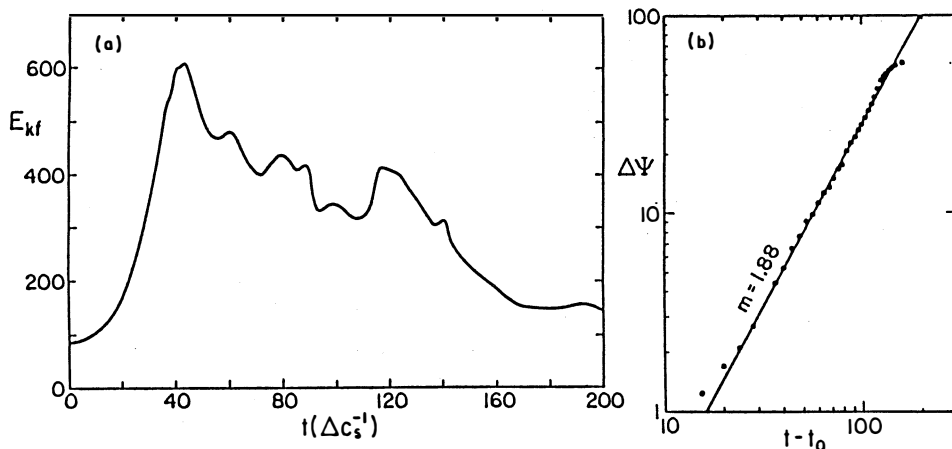
Fig. 7. Temporal profiles of the fluid energy (a) and the reconnected flux (b) for $\epsilon_c = 0.7$ obtained from the MHD particle simulation. A solid line in (b) is a fit to the observation.

also less in present case. The case with $\epsilon_c = 0.3$ was treated, where $\Delta\psi \propto t^m$ with m=1. Thus, it is clear that as ϵ_c increases, the process of reconnection becomes faster, changing from the Sweet-Parker rate to the Brunel-Tajima rate to the explosive rate. It is also remarkable that the explosive increase of reconnected flux during the coalescence is observed in the MHD simulation as well as in the kinetic simulation discussed earlier.

The structure and its evolution of the plasma and magnetic fields during the coalescence are examined.

These signatures are consistent with our hypothesis (a) that the reconnection takes place by the mechanism of Sweet and Parker for coalescence with $\epsilon_c = 0.3$. The signatures found in $\epsilon_c = 0.3$, on the other hand, imply that the reconnection process is not that of Sweet and Par-Parker. It shows instead that (1) the reconnection angle at the x-point has enlarged; (2) a high density spot near the x-point is formed; (3) the reconnected flux increases faster than the Sweet-parker process ($\Delta\psi \propto t^m$ with m ~ 2). These are consistent with our further hypotheses (b) that the reconnection is through the process of Brunel, Tajima and Dawson for coalescence with $\epsilon_c = 0.7$. Later (t=160), the system approaches saturation when most of the the flux available has reconnected as seen in $\epsilon_c = 0.7$ (at t=140 for this frame) and the high density region shifted from the x-point to the coalesced island hedge. The flow is randomized.

To supplement our kinetic simulation in order to make comparison with the MHD particle simulation, we present a run starting from the Faddeev equilibrium. In this case the equilibrium is the same as the MHD particle run, although the parameters such as the collisionless skin depth are different because of the difference in model.

Figure 8 presents the pattern of the plasma and fields of the case $\epsilon_c = 0.85$, where we see faster and explosive reconnection (Fig. 6). We are advancing our third hypothesis (c) that the coalescence with $\epsilon_c = 0.85$ is explosive whose reconnection process is to be characterized by the present paper. In frames of Figs. 8 (a) − (d) (t=50) one sees the coalescence behavior be-fore it becomes explosive. Although, in Figs. 8(a) and (b), in particular, one can detect some deviation from the Sweet-Parker type for $\epsilon_c = 0.3$, it is qualitatively similar to the $\epsilon_c = 0.3$ case
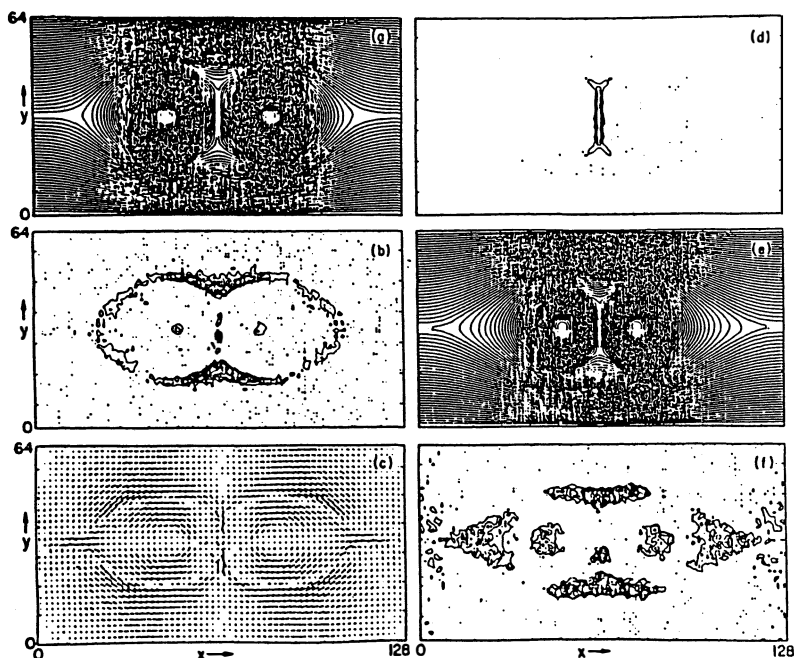
Fig. 8. Spatial structure of plasma and fields "before" and "during" coalescence with $\epsilon_c = 0.85$. (a) Magnetic field lines. (b) Plasma density contours. (c) Plasma flow velocities. (d) Current density (J_z) contours. (a)-(d) at $t = 50 \Delta c_s^{-1}$. (e) Magnetic field lines. (f) Plasma density contours. (e) and (f) at $t = 87.5 \Delta c_s^{-1}$.

and the $\epsilon_c = 0.7$ case at this stage. In Figs. 8 (e) and (f) (t=75), we now see significant deviations in pattern from the cases with less $\epsilon_c = 0.7$. A much wider reconnectigon angle than the previous ones is observed in Fig. 8 (e). From these observations it can be argued that the widening of the reconnection angle has to be accmopanied by fast or explosive coalescence.

2,2, Theoretical Model of Explosive Coalescence

As shown in the previous section, the current sheet of nearly one-dimensional structure is formed in the explosive stage of the coalescence instability. As the coalescence proceeds further, the magnetic field structure approaches an x-type (Petsheck type) configuration. We assume that $\partial/\partial x >> \partial/\partial y$, $\partial/\partial z$, in which x is the direction of coalescence, while y is the direction of poloidal magnetic field line and z is the direction of plasma current. We treat the external plasma dynamics of the explosive stage as a one-dimensional problem.

As we shall see in our separate paper (Tajima and Sakai, 1985), in one-dimensional limiting case of two-dimensions, we get essentially the same results as we obtain in this section.

we start from the two-fluid model equations of plasma and the Maxwell equations, neglecting the displacement current. We assume the adiabatic law of states for both electrons and ions. The basic equations read as follows:

$$\frac{\partial n_j}{\partial t} + \nabla \cdot (n_j v_j) = 0 \tag{1}$$

$$m_j n_j \frac{d\mathbf{v}_j}{dt} = n_j e_j \left(\mathbf{E} + \frac{\mathbf{v}_j}{c} \times \mathbf{B} \right) - \nabla p_j, \tag{2}$$

$$\nabla \times \mathbf{B} = \frac{4\pi}{c} \sum_j n_j e_j \mathbf{v}_j, \tag{3}$$

$$\nabla \cdot \mathbf{E} = 4\pi \sum_j n_j e_j, \tag{4}$$

$$\nabla \times \mathbf{E} = -\frac{1}{c} \frac{\partial \mathbf{B}}{\partial t}, \tag{5}$$

$$\frac{\partial p_j}{\partial t} + \mathbf{v}_j \cdot \nabla p_j + \gamma p_j \operatorname{div} v_j = 0, \tag{6}$$

where j denotes the species of particles and γ is the ratio of heat capacity which is related to the degree of freedom of the system f as $\gamma = 1 + 2/f$.

During coalescence, there is no specific scale length. The scale length characterizing the current sheet varies continuously in time without deformation of global structure of current sheet. If one looks at the evolution of the system locally in time (in the neighborhood of $t = t_s$), the system undergoes the rapid field and temperature swelling, compression of plasma and the size of the current sheet, change of the reconnection angle etc. in a certain specific fashion which was detailed in Sec. 2. If one looks at the same system locally in time a little later (in the neighborhood of $t = t_s + t_s^1$), the system undergoes these changes with differrent magnitudes, but still in the same specific fashion. That is, the relations (laws) that govern the explosive coalescence themselves are invariant under the change of time scale. This was the manifestation of the presence of self-similarity in the system during explosive coalescence.

Such a physical situation may best be described by self-similar soulutions in which scale factors vary continuously. We introduce scale factors $a(t)$ and $b(t)$ as follows,

$$v_{ex} = \frac{\dot{a}}{a} x, \tag{7}$$

$$v_{ix} = \frac{\dot{b}}{b} x, \tag{8}$$

where a dot represents the time derivative. An ansatz is imposed here that the velocities are linear in x. The linear dependence on x of the velocity implies that ions and electrons stream in the opposite direction around the center of current sheet, $x = 0$. The scale factors a and b will be determined from the above basic equations. From the continuity equations of electrons and ions, Eq. (1), we obtain

$$n_e = n_0 / a, \tag{9}$$

$$n_i = n_0 / b, \tag{10}$$

where n_0 is a constant. Equations (9) and (10) show that the densities of ions and electrons are nearly homogeneous in space and vary only in time during coalescence. The self-similar solutions obtained here are local solutions in space whose physical process dominates near the current sheet. We therefore neglect the higher order terms in space proportional to x^3 and higher hereafter. The current J_z in the sheet is nearly constant. This means that as n_j is nearly

constant, v_{zj} is also approximately constant in space. Neglecting the term with x^3 in Eq. (3), we obtain

$$\frac{B_0(t)}{\lambda} = \frac{4\pi e n_0}{c} \left(\frac{v_{iz}^{(0)}}{b} - \frac{v_{ez}^{(0)}}{a} \right), \tag{11}$$

where we assumed the magnetic-field B_y varies as $B_y = B_0 (t)\frac{x}{\lambda}$, where λ is the magnetic field scale length. This ansatz is consistent with the assumption that the sheet current is constant in space.

From the y-component of Eq. (5) and the z-component of the equation of motion for electrons Eq. (2) we obtain

$$\dot{B}_0 = 2c\frac{E_{z1}}{\lambda}, \tag{12}$$

$$E_{z1}\frac{x^2}{\lambda^2} + \frac{\dot{a}}{a}\frac{B_0(t)}{\lambda c} x^2 = 0, \tag{13}$$

$$\frac{\partial v_{ez}^{(0)}}{\partial t} = -\frac{e}{m_e} E_{z0}, \tag{14}$$

where

$$E_z = E_{z0}(t) + E_{z1}(t)\frac{x^2}{\lambda^2}.$$

Equations (12) and (13) yield

$$B_0(t) = \frac{B_{00}}{a^2}, \tag{15}$$

where B_{00} is a constant. From the z-component of the equation of motion for ions, we get

$$\frac{\partial v_{iz}^{(0)}}{\partial t} = \frac{e}{m_i} E_{z0}. \tag{16}$$

From Eqs. (14) and (16) we have

$$v_{iz}^{(0)} = -\frac{m_e}{m_i} v_{ez}^{(0)}. \tag{17}$$

From Eqs. (15), (17) and (11), we get for $v_{ez}^{(0)}$ aund E_z

$$v_{ez}^{(0)} = -\frac{cB_{00} b}{4\pi e n_0 \lambda a^2 \left(\frac{b}{a} + \frac{m_e}{m_i}\right)}, \tag{18}$$

$$E_z = -\frac{B_{00}\dot{a}x^2}{ca^3\lambda} + \frac{m_e c B_{00}}{4\pi n_0 e^2 \lambda}\frac{d}{dt}\left(\frac{b}{a^2\left(\frac{b}{a} + \frac{m_e}{m_i}\right)}\right). \tag{19}$$

Assuming that the electrostatic field E_x varies like $E_x = E_0(t) x/\lambda$, we obtain from Poisson's equation (4)

$$E_0 = 4\pi e n_0 \lambda \left(\frac{1}{b} - \frac{1}{a}\right). \tag{20}$$

Furthermore, the equations of state for electrons and ions give rise to

$$P_e = \frac{P_{0e}}{a^\gamma} - \frac{P_{0e}}{2a^{\gamma+2}}\frac{x^2}{\lambda^2}, \tag{21}$$

$$P_i = \frac{P_{0i}}{b^\gamma} - \frac{P_{0i}}{2b^{\gamma+2}}\frac{x^2}{\lambda^2}. \tag{22}$$

We now go back to the x-component of the equations of motions for electrons and ions in order to obtain the basic equations for $a(t)$ and $b(t)$. If we neglect the small terms of the order

of the mass ratio m_e/m_i, we obtain

$$\ddot{a} = -\omega_{pe}^2 \left(\frac{a}{b} - 1 \right) - \frac{B_{00}^2}{4\pi m_e n_0 \lambda^2 a^2} + \frac{P_{0e}}{m_e n_e \lambda^2 a^\gamma} \quad , \tag{23}$$

$$\ddot{b} = \omega_{pi}^2 \left(1 - \frac{b}{a} \right) + \frac{P_{0i}}{m_i n_0 \lambda^2 b^\gamma} \quad . \tag{24}$$

Furthermore, assuming that the plasma is quasi-neutral $n_i = n_e$, i.e., a = b, by adding Eqs. (23) and (24)

$$\ddot{a} = -\frac{v_A^2}{\lambda^2 a^2} + \frac{c_s^2}{\lambda^2 a^\gamma} \quad , \tag{25}$$

where

$$v_A^2 = \frac{B_{00}^2}{4\pi n_0 (m_i + m_e)} \quad \text{and} \quad c_s^2 = \frac{(P_{0e} + P_{0i})}{(m_e + m_i) n_0} \quad .$$

In Eg.(25) the first term of the RHS corresponds to the J x B term. This is the term that drives magnetic collapse. The secound term corresponds to the pressure gradient term. This term may eventually be able to balance the magnetic compression (collapse) when $\gamma = 3$. The condition $\gamma = 3$ means that the plasma compression takes place in a nearly one-dimensional fashion so that the degree of freedom of the system becomes unity. When $\gamma = 3$, we obtain

$$\ddot{a} = -\frac{v_A^2}{\lambda^2 a^2} + \frac{c_s^2}{\lambda^2 a^3} \quad . \tag{26}$$

When $\gamma = 2$ (f = 2), on the other hand, we obtain

$$\ddot{a} = -\frac{(v_A^2 - c_s^2)}{\lambda^2 a^2} \quad . \tag{27}$$

Once the behavior of the scale factor a(t) is determined from the above equations, we obtain various kinds of physical quantities as fllows, in the quasi-neutral plasmas, and neglecting the mass ratio ($m_e/m_i \to 0$),

$$B_y = \frac{B_{00}}{a^2} \frac{x}{\lambda} \tag{28}$$

$$E_x = \left(-\frac{m_i v_A^2}{e\lambda a^3} + \frac{P_{0e}}{e\lambda a^4 n_0} \right) \frac{x}{\lambda} \tag{29}$$

$$E_z = -\frac{B_{00} \dot{a} x^2}{ca^3 \lambda} - \frac{B_{00} m_e c\dot{a}}{4\pi n_0 e^2 \lambda a^2} \tag{30}$$

$$v_{ez} = -\frac{cB_{00}}{4\pi e n_0 \lambda a} \tag{31}$$

$$v_{ix} = v_{ex} = \frac{\dot{a}}{a} x \tag{32}$$

$$n_i = n_e = \frac{n_0}{a} \tag{33}$$

where the electrostatic field E_x in the quasi-neutral plasmas is determined from the equation of motion for ions, not from Poisson's equations.

Frgom Egs. (28) and (29) we find the important result that in the explosive phase (a→0) the electrostatic field $E_x \propto (a^{-3} + a^{-4})$ grows more rapidly than the magnetic field ($B_y \propto a^{-2}$) does. This effect plays a pivotal role for high energy particle production.

Now we investigate the global time bcehavior of coalescence by making use of the first integral of Eq. (26). Equation (26) may be rewritten as

$$\ddot{a} = -\frac{\partial V(a)}{\partial a} \quad , \tag{34}$$

where the effective (Sagdeev) potential $V(a)$ is given by

$$V(a) = -\frac{v_A^2}{\lambda^2 a} + \frac{c_s^2}{2\lambda^2 a^2} , \tag{35}$$

where the first term may be reminiscent of the "gravitational potential", while the second of the "centrifugal potential." The schematic graph of the effective potential is drawn in Fig. 9. The value a which satisfies $V(a_1) = 0$ is given by
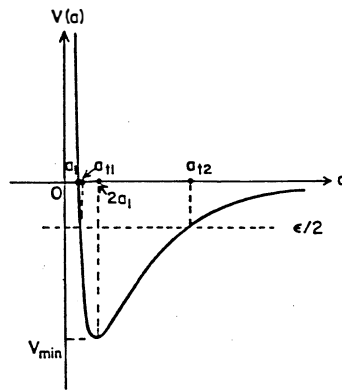

Fig. 9. The Sagdeev potential for the scale factor of the explosive coalescence.

$$a_1 = \frac{1}{2}\frac{c_s^2}{v_A^2} \quad . \tag{36}$$

The minimum of the potential, V_{min}, obtained from $\partial V / \partial a = 0$ is

$$V_{min} = \frac{-v_A^4}{2\lambda^2 c_s^2} , \tag{37}$$

at $a = 2a_1 = c_s^2 / v_A^2$. The potential becomes deeper when the ratio of the kinetic to magnetic energy densities $\beta = c_s^2 / v_A^2$ approaches zero. This means that the driving force $J \times B$ is dominant compared with the pressure term. The first intgegral of Eq. (34) is given by

$$\dot{a}^2 = \frac{2v_A^2}{\lambda^2 a} - \frac{c_s^2}{\lambda^2 a^2} + \varepsilon , \tag{38}$$

where ε is the initial (Sagdeev) "energy" (dimension: $1/time^2$) in space of stretching factor a.

$$\varepsilon = \dot{a}_0^2 - \frac{2v_A^2}{\lambda^2 a_0} + \frac{c_s^2}{\lambda^2 a_0^2} . \tag{39}$$

As seen from Fig. 9 , the explosive magnetic compression corresponds that the scale factor $a(t)$ rapidly changes in time by orders of magnitude and vanishes. We may call this an ex- explosive magnetic collapse. Such an explosive collapse can be realized (1) when the effective potential has a sharp and deep potential well and this means that $\beta = c_s^2 / v_A^2$ is very small; (2) when the initial total energy $\varepsilon / 2$ is nearly zero. On the other hand, when $\varepsilon / 2$ is close to $-v_{min}$, we have oscillations near the potential minimum and no explosive

collapse.

If the total energy is given in Eq.(38), we can find the period T of nonlinear oscillations by integrating Eq. (38)

$$T_{os} = 2 \int_{a_{t1}}^{a_{t2}} \frac{a\,da}{\left[\varepsilon \left(a + \frac{v_A^2}{\varepsilon \lambda^2} \right)^2 - \frac{v_A^2}{\varepsilon \lambda^2} - \frac{c_S^2}{\lambda^2} \right]^{1/2}}$$

$$= 2\pi \frac{v_A^2}{\varepsilon^{3/2} \lambda^2} = 2\pi \varepsilon^{-3/2} t_A^{-2}, \tag{40}$$

where a_{t1}, a_{t2} are roots of the equation which gives $\dot{a} = 0$:

$$a^2 + \frac{2v_A^2}{\varepsilon \lambda^2} a - \frac{c_S^2}{\varepsilon \lambda^2} = 0, \tag{41}$$

and $t_A = \lambda/v_A$. In the limit of $\varepsilon \to -v_{min}$, we find the minimum period T_{min} as

$$T_{min} = 2\pi \beta^{3/2} t_A. \tag{42}$$

Equation (40) indicates that the period T_{os} of nonlinear oscillations becomes longer when ε tends to zero.

Let us examine the time history of various physical quantities based in the qualitative time behavior of a (t) derivable from the effective potential $V(a)$. The magnetic field energy is proportional to B_y^2, which is given by

$$B_y^2 = \frac{B_{00}^2}{a^4} \left(\frac{x}{\lambda} \right)^2.$$

If the scale factor a becomes smaller, B_y^2 must increase. The maximum is given by

$$\frac{\partial B_y^2}{\partial t} = 0,$$

which yields $\dot{a} = 0$, namely $a = a_{t1}$. After the maximum, B_y^2 decreases again and reaches a minimum at $a = a_{t2}$. The oscillatory behavior of the magnetic field energy is schematically drawn in Fig. 10. The period of the oscillation is given by Eq.(40).
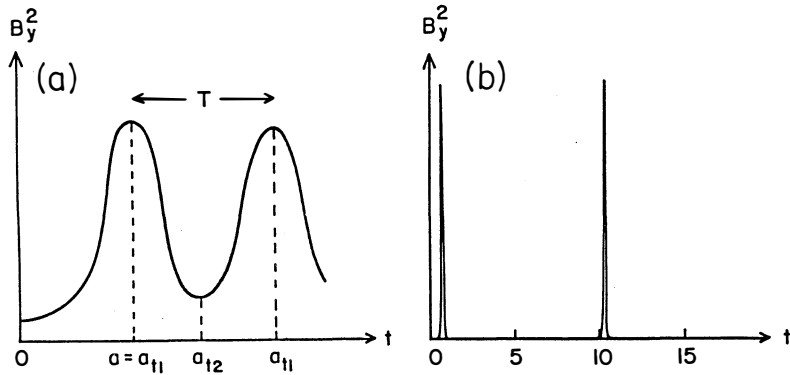

Fig. 10. The temporal behavior of the magnetic field energy constructed from the Sagdeev Potential (a) and numerical result (b).

The electrostatic field E_x is given by Eq. (29). The time history of the electrostatic field energy, which is proportional to E_x^2, is analyzed by investigating

$$\frac{\partial E_x^2}{\partial t} = 0 .$$

This condition is equivalent to

$$\epsilon_0 = 0, \tag{43}$$

or

$$\frac{\partial \epsilon_0}{\partial t} = 0, \tag{44}$$

where $\epsilon_0 (t) = -\dfrac{m_i v_A^2}{e \lambda a^3} + \dfrac{P_{0e}}{e \lambda n_0 a^4}$. The first condition $\epsilon_0 = 0$ occurs at $a = a_3 = P_{0e} / m_i n_0 v_A^2 = c_s^2 / v_A^2$. The second condition $\partial \epsilon_0 / \partial t = 0$ gives two conditions, namely

(ii) $\dot{a} = 0$, which occurs at $a = a_{t1}$, a_{t2}

(ii) $a = a_4 = \dfrac{4}{3} \dfrac{P_{0e}}{m_i n_0 v_A^2} \cong \dfrac{4}{3} \dfrac{c_s^2}{v_A^2}$.

The above considerations give us the schematic time history of the electrostatic field energy E_x^2 as drawn in Fig. 11. Figure 11 indicates a triple-peak structure in the electrostatic
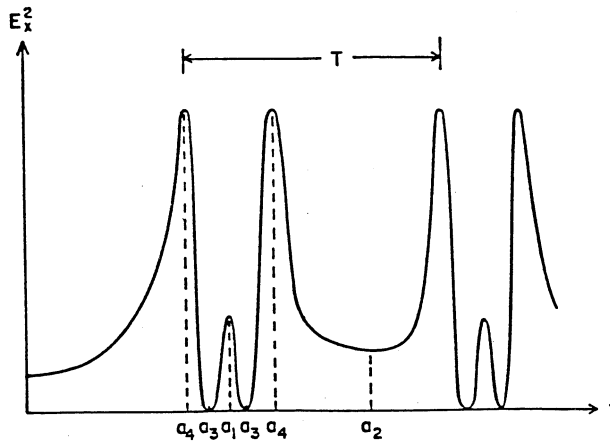

Fig. 11. The temporal behavior of the electrostatic field energy constructed from the Sagdeev potential.

field energy. When the plasma β is small, a_3, a_{t1} are close. In this case, the triple-peak structure in the electrostatic field energy would become double-peak structure. The maximum value of the electrostatic field, E_{max}, achieved at $a = a_4$ is given by

$$E_{max} = \frac{1}{4} \left(\frac{3}{4} \right)^3 \frac{m_i}{e \lambda} \frac{v_A^8}{c_s^6} \frac{x}{y} \cong 0.1 \frac{m_i}{e \lambda} \frac{v_A^2}{\beta^3} \frac{x}{y} . \tag{45}$$

The induced elecstric field E_z is given by Eq. (30), which shows that E_z becomes zero, when $\dot{a} = 0$. E_z changes its sign around $\dot{a} = 0$ because $\dot{a} = 0$ is the point where the magnetic field achieves maximum or minimum.

Next, the time behavior of ion temperrature T_{ix} is examined. In the early stage of coalescence, the plasma should be adiabatically compressed. However, as the magnetic field energy increases near the peak and approaches the peak, the ion flow energy becomes dominant

over the thermal energy. From the consideration that v_x^2 gives maximum or minimum, namely $\dfrac{\partial v_x^2}{\partial t} = 0$, we find two conditions for the extrema; (i) $v_x = 0$, which gives $\dot{a} = 0$, (ii) $\dfrac{\partial v_x}{\partial t} = 0$, which gives

$$a\ddot{a} = \dot{a}^2 . \tag{46}$$

When the explosive coalescence takes place ($\varepsilon = 0$), we estimate the conditigon (46) as

$$a = a_5 \cong \frac{2}{3} \frac{c_s^2}{v_A^2} .$$

After a = a_5, the kinetic energy must decrease, which means that the plasma is in the state of the colliding phase. The above considerations give us the schematic time history of the ion temperature, which is shown in Fig. 12. Figure 12 shows a double-peak structure in the ion
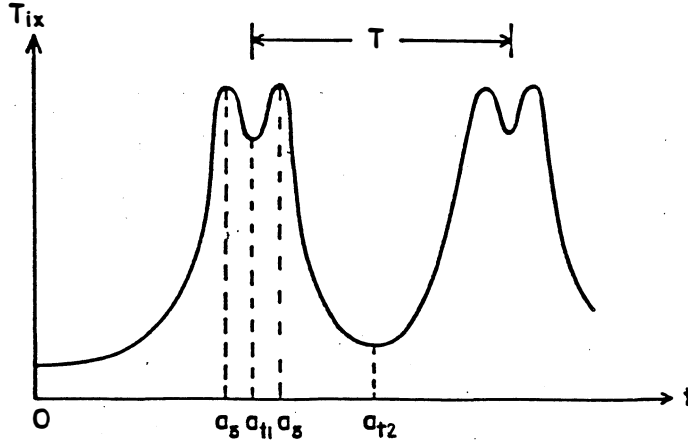

Fig. 12. The temporal behavior of the ion-temperature in the x-direction (in the direction of coalescence) constructed from the Sagdeev potential.

temperature. In the limit of quasi-neutrality, we can estimate the dominant term governing the explosive phase where the adiabatic compression is predominant. The temperature T is given by T = P / n, while the dominant term in prerssure changes in time as $P \sim a^{-5}$ when $\gamma = 3$, $P \sim a^{-4}$ when $\gamma = 2$, while $n \sim a^{-1}$. Therefore we find

$$T = P/n \cong \frac{1}{a^4} \quad (\gamma = 3) \tag{47}$$

$$\cong 1/a^3 \quad (\gamma = 2). \tag{48}$$

We investigate in more detail the explosive phase of the coalescence in the case where we can neglect the effect of plasma pressure: it only acts as a saturation mechanism. However, if we take $\gamma = 2$, the pressure does not take the role of a saturation mechanism as seen in Eg. (27). In the explosive phase, therefore, we can neglect the second term in the right-hand side of Eq. (26);

$$\ddot{a} = -\frac{v_A^2}{\lambda^2 a^2} \tag{49}$$

Furthermore, we need a second condition for explosive collapse, namely the initial total

energy must be close to zero, For example, if the oscillation period of magnetic energy is of the order of the transit Alfven time $t_A = \lambda / v_A$, we can estimate the total energy ε by making use of Eq. (40) as

$$T_{os} = 2\pi\varepsilon^{-3/2} t_a^{-2} \cong t_A , \tag{50}$$

which gives

$$\varepsilon \sim \frac{(2\pi)^{2/3}}{t_A^2} \tag{51}$$

The solution of Eq. (49) with small ε is given by

$$a(t) \cong \left(\frac{9}{2}\right)^{1/2} \left(\frac{v_A}{\lambda}\right)^{2/3} (t_0 - t)^{2/3} + 0(\varepsilon) , \tag{52}$$

where we neglect the order of ε, and t_0 is the explosion time. Once the solution $a(t)$ is given by Eq. (52), we can find the various physical quantities by following, whicn is valid in the explosive phase of the coalescence;

$$v_x = v_{ix} = v_{ex} = -\frac{2}{3}\frac{x}{(t_0 - t)} , \tag{53}$$

$$n = n_i = n_e = \left(\frac{2}{9}\right)^{1/3} \frac{\lambda^{2/3} n_0}{v_a^{2/3} (t_0 - t)^{2/3}} , \tag{54}$$

$$E_x = -\frac{2}{9}\frac{m_i}{e}\frac{x}{(t_0 - t)^2} , \tag{55}$$

$$B_y = \left(\frac{2}{9}\right)^{2/3} \frac{B_{00} \lambda^{1/3} x}{v_a^{4/3} (t_0 - t)^{4/3}} , \tag{56}$$

$$E_z = \frac{2}{3}\left(\frac{2}{9}\right)^{2/3} \frac{B_{00} \lambda^{1/3} x^2}{v_A^{4/3} c(t_0 - t)^{7/3}} + \frac{2}{3}\left(\frac{2}{9}\right)^{1/3} \frac{B_{00} c}{\omega_{Pe}^2 \lambda^{1/3} v_a^{2/3} (t_0 - t)^{5/3}} . \tag{57}$$

The explosion time t_0 is related to the initial condition. From Eq. (53) we find the initial velocity v_{x0} at $t = 0$ as

$$v_{x0} = \frac{\dot{a}_0}{a_0} x = -\frac{2x}{3t_0} , \tag{58}$$

where a_0, $\dot{a}_0$ are the initial values of a, $\dot{a}$ at $t = 0$. From Eq. (58) we find

$$t_0 = -\frac{2}{3}\frac{a_0}{\dot{a}_0} \quad (>0) , \tag{59}$$

where $\dot{a}_0$ must be negative when magnetic collapse occurs. On the other hand, a_0 and $\dot{a}_0$ are related to the initial total energy as

$$\varepsilon = \dot{a}_0^2 - \frac{2 v_A^2}{\lambda^2 a_0} \tag{60}$$

when the pressure term is neglectged. If $\varepsilon \to 0$, we obtain from Egs. (59) and (60)

$$t_0 \cong \frac{\sqrt{2}}{3} a_0 \sqrt{a_0} t_A . \tag{61}$$

Combining Eqs. (55) and (56), we find the important result that in the explosive phase the electrostatic field $E_x \propto (t_0 - t)^{-2}$ more rapidly grows compared with the magnetic frield $B_y \propto (t_0 - t)^{-4/3}$. This fact becomes very important when we consider the high energy particle production by E_x during the explosive phase of the coalescence.

Let us compare the theoretical results obtained here for the explosive phase with the computer simulation results. The global structure of the magnetic field energy, electostatic field energy, ion temperature in the x-direction observed in the simulation is well explained by the theoretical model obtained here. Especially, the double-peak structure in the ion temperature, and the triple-peak structure in the electrostatic field energy are also observed in the simulation (see Figs. 1 and 2). Table 1 summarizes the results of comparison between the theory and the collisionless simulation.

In Table 1 we show the index m of explosiveness (the exponent to the time $(t_0 - t)^{-m}$).

TABLE I
Indices of Explosion [exponents to the $1/(t_0 - t)$] During Coalescence

		$\Omega_{et} = 0$ $L_x \times L_y$ $= 128 \times 32$ (see Ref. 26) [NB: $L_x \times L_y$ $= 256 \times 32$ many islands]	$\Omega_{et} = 0.2\,\omega_{pe}$ $L_x \times L_y$ $= 128 \times 32$	$\Omega_{et} = 1.0$ $L_x \times L_y$ $= 128 \times 32$	$\Omega_{et} = 2.0$ $L_x \times L_y$ $= 128 \times 32$ No formation of islands
Magnetic Energy B^2	(S)	8/3	8/3	2	
	(T)	8/3	8/3	2 *	N/A
Electrostatic Energy E_l^2	(S)	4	4		
	(T)	4	4	4	N/A
Ion Temperature in x-direction T_{ix}	(S)	8/3	8/3	3	
	(T)	8/3	8/3	2	N/A
Explosive Time t_0	(S)	$24.3\Omega_i^{-1}$	$27\Omega_i^{-1}$	$19\Omega_i^{-1}$	N/A
Compressional Alfvén Oscillation Period τ_{os}		$6.3\Omega_i^{-1}$	$6.0\,\Omega_i^{-1}$	$8.8\,\Omega_i^{-1}$	N/A

* incompressibility is assumed. Derivation from observation might be due to plasma rotation in $\Omega_{et} = 1$ case.

S is for simulation results and T for theory.

Table 1 shows a good agreement between simulation and theory in the electrostatic energy. When the toroidal field becomes comparable to the poloidal field ($B_T / B_P = 1$ case), there appears two-dimensional motion, plasma rotational motion, which makes a more complex

electrostatic field configuration. When $B_T / B_P = 1$, the magnetic time behavior of field energy also deviates from the one-dimensional analysis for the same reason. For the ion temperature we find its explosiveness from Eq. (47) as

$$T \sim \frac{1}{a^4} \sim \frac{1}{(t_0 - t)^{8/3}} \tag{62}$$

when $\gamma = 3$. The above scaling also is close to the results obtained in the simulation, except for the case of $B_T / B_P = 1$.

Figure 13 shows the spectral intensity $S(k, \omega)$ obtained from the simulation run that
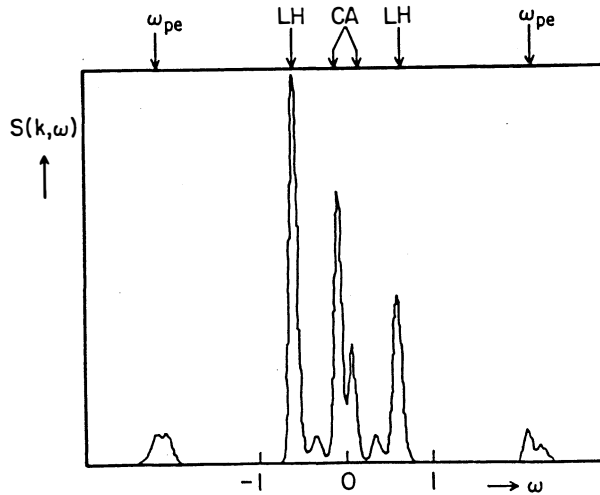

Fig. 13. Radiation spectrum during explosive current loop coalescence.

corresponds to Fig. 2. Since the spectral intensity is integrated over time, the most intense period of various modes is most heavily weighted. For most modes this intense period corresponds to that after the coalescence. Thus, it becomes necessary to recalibrate the plasma density and magnetic field strength, etc. at that stage. These recalibrated eigenfrequencies are indicated near the edge of the frame of Fig. 13. We observe that the lower hybrid range frequency contains strongest spectral intensity, followed by the compressional Alfvén modes that correspond to the coalescence and ensuing oscillations, and the plasma oscillations ($\omega \cong \omega_{Pe}$). The frequency happens to be outside of the frame so that we do not know if they are prominent or not.

Finally. comments in the effect of non-quasineutrality are due. In the explosive phase. we can neglect the effect of pressure terms in Eq. (23) and Eq. (24):

$$\ddot{a} = -\omega_{Pe}^2 \left(\frac{a}{b} - 1 \right) - \frac{v_{Ae}^2}{\lambda^2 a^2}, \tag{63}$$

$$\ddot{b} = \omega_{Pi}^2 \left(1 - \frac{b}{a} \right). \tag{64}$$

From the analysis of numerical calculations of Eqs. (63) and (64), we can conclude that b is slowly varying in time during the variation nf a. Therefore if we use the result $b \cong b_0 = $const. in Eq. (63), we find the effective potential $V(a)$ as

$$\ddot{a} = -\frac{\partial V(a)}{\partial a} \ ,$$

$$V(a) = \omega_{pe}^2 \left(\frac{a^2}{2b_0} - a \right) - \frac{v_{Ae}^2}{\lambda^2 a} \ , \tag{65}$$

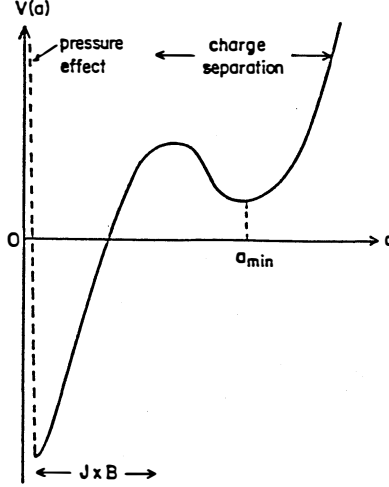The schematic graph of the potential is given in Fig. 14. Here we write the effective

Fig. 14. The Sagdeev potential for the scale factor including the plasma pressure.

potential including the effect of plasma pressure. The curve that incorporates the pressure effect is shown as the broken line near a =0. Figure 14 shows a second minimum at a = a_{min} which is caused by the effect of charge separation. When the J x B force dominates, the charge separation effect is unimportant . Such is the case of explosive phase of coalescence (where charge neutrality is maintained to a good degree). However, after the coalescence in the late stage of amplitude oscillations, the J x B force becomes weaker. Then the charge separtion may become important. In this stage electrons can be trapped and oscillate in the potential well near the second minimum in Fig. 14. The electrostatic field oscillations are similar to the dipole oscillations near the current sheet. Such dipole oscillations may be able to radiate the electromagnetic wave ($\omega \sim \omega_{pe}$ or ω_{pi}), if the plasma is not evanescent. The simulation results obtained show certain high freguency oscillations in the frequency range of $\omega \sim \omega_{pe}$, ω_{LH} . The detailed comparison will be reoported elsewhere. Once other effects such as the two-dimensional curvature effect are included, it might be possible to have additional minima in the effective potential and thus for the system to be temporarily trapped in the potential well and exhibit pulsations.

We have found that in the explosive phase of magnetic collapse the electrostatic field can be explosively generated and grow more rapidly than the magnetic field.

The explosiveness of the electrostatic field $E_x \sim (t_0 - t)^{-2}$, and magnetic field $B_y \sim (t_0 - t)^{-4/3}$ well agree with the results obtained in the simulations (see Fig. 1) As shown later, the kinetic simulation finds that in the explosive phase ions and electrons are simultaneously accelerated in the z-direction, opposite to each other. When a particle moves across the magnetic field driven by the electrostatic field E the particle can be accelerated in the

direction (z-direction) perpendicular both to the electric field (x-direction) and the poloidal magnetic field (y-direction). This acceleration mechanism was considered by Sugihara and Mizuno (1979). On the other hand, Sagdeev and Shapiro discussed the same physics in another point of view, namely the large amplitude wave damping due to trapped electrons. These previous works are applicable to the cases in which the large amplitude electrostatic waves can propagate across the static magnetic field. In the explosive phase during magnetic collapse, a similar situation can be realized; now the magnetic field and electrostatic field can vary in time and space.

Figure 15 shows the distribution functions of electrons and ions in the coalescence simulation from the electromagnetic particle code. In Fig. 15 we compare the distribution of elect-
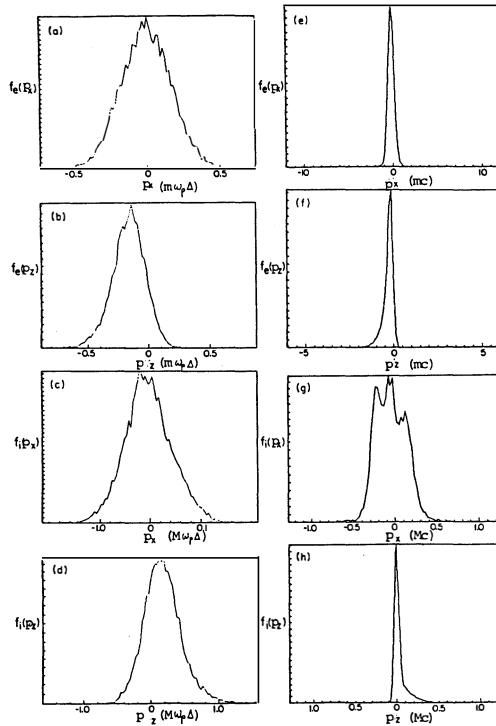

Fig. 15. Distribution functions of electrons and protons before coalescence (a)-(d) and after coalescence (e)-(h).

rons and ions before the explosive coalescence with the distribution after that.

It is clear that the distribution functions have very rapidly changed during the explosive coalescence and strong heating of ions in the coalescence direction has occurred during this time. It is also observed that there is a very small but energetic population of electrons has been created in the z-direction perhaps due to the inductive acceleration. A similar pattern is observed in the ion distribution in the z-direction with the appropriate parity difference because of the charge difference between electrons and ions. It should be noted that the explosive coalescence produces extremely energetic ions which form a relatively flat and long plateau.

3. Current Loop Coalescence in Solar Flares

Recent observations of x-ray continuum emission, γ-ray line, and continuum emission from rsolar flares with instruments on the Solar Maximum Mission (SMM) and Hinotori satellites show that energetic ions and relativistic electrons are accelerated almost simultaneously with non-relativistic electrons during the impulsive phase of solar flares. These observational results make it necessary to revise the widely accepted hypothesis of particle acceleration that energetic ions and relativistic electrons asre produced in the second phase a few minnutes after the impulsive phase (Wild et al., 1963; de Jager, 1969; Svestka, 1976). Although Bai and Ramaty (1979), Bai (1982), and Bai et al. (1983) revised the hypothesis as the secondstep acceleration taking note of a small delay of γ-ray line emission from hard x-ray emission, Kane et al. (1983), and Forrest aund Chupp (1983) pointed out that such a small delay can be explainced simply by either the injection, propagaztion, or energy loss processes of particles which are accelerated in a single step.

Recently Nakajima et al. (1983) and Kiplinger et al. (1983) reported observations of qubasi-periodic pulses with double subpeak structure seen in hard x-ray, γ-ray and microwave emissions in the two intense solar flares of June 7, 1980 and June 21, 1980. We are interested in the close similarity between the observed time profiles and those obtained with the computer simulation given in the previous section.

We present the results of our analysis of the June 7, 1980 and November 26, 1982 events, both of which are widely different from each other in duration, source size, source height, etc., they provide a stringent test for examining the validity of our model of particle acceleration in solar flares in terms of the coalescence instability. Our study shows that observational features of the two events are consistent with the results of our ecomputer simulation.

3.1 Summary of observations

(a) June 7, 1980 Event

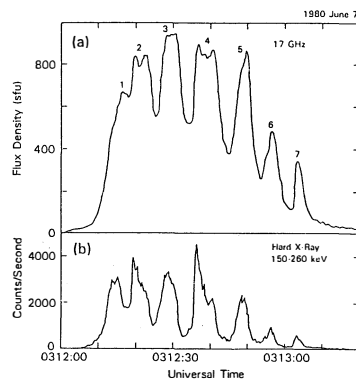The impulsive burst of the June 7, 1980 solar flare (Fig. 16) has been investigated by

Fig. 16. Time profiles of 17 GHz microwave and 150−260 kev X-ray emissions (from the Hard X-ray Burst Spectrometer on SMM) of June 7, 1980 Flare.

many authors (Forrest et al., 1981; Kane et al., 1983; Forrest and Chupp, 1983; Nakajima et al., 1983; Kiplinger et al., 1983). We summarize below some essential points from these observations.

(1) The burst is composed of seven successive pulses with a quasi-periodicity of about 8 seconds. Each of the pulses in hard x-rays, prompt γ-ray lines, and microwave is almost synchronous and similar in shape.

(2) The microwave pulses consist of double sub-peaks as seen especially in the second and fourth pulses in Fig. 16(a).

(3) The starting times of hard x-rays, prompt γ-ray lines, and microwaves coincide within ±2.2 seconds.

(4) The time scales of acceleration for both electrons (up to energies above 1 MeV) and ions (above 10 MeV/nucleon) are less than 4 seconds. The accelerations must occur almost simultaneously.

(5) The height of the microwave source is estimated to within 10 are sec above the photosphere (H_α flare; N12, W64). The source has asmall size of less than 5 are sec in the east-west direction and shows no motion.

The H_α photographs from the Peking Observatory (H. Chow, private communication) add a new finding. The flaring region has two structures that appear to be in contact with each other, one stretching in the east-west direction and the other in the north-south.

(b) November 26, 1982 Event

We briefly outline the characteristics of the Nobember 26, 1982 flare (Fig. 17). This
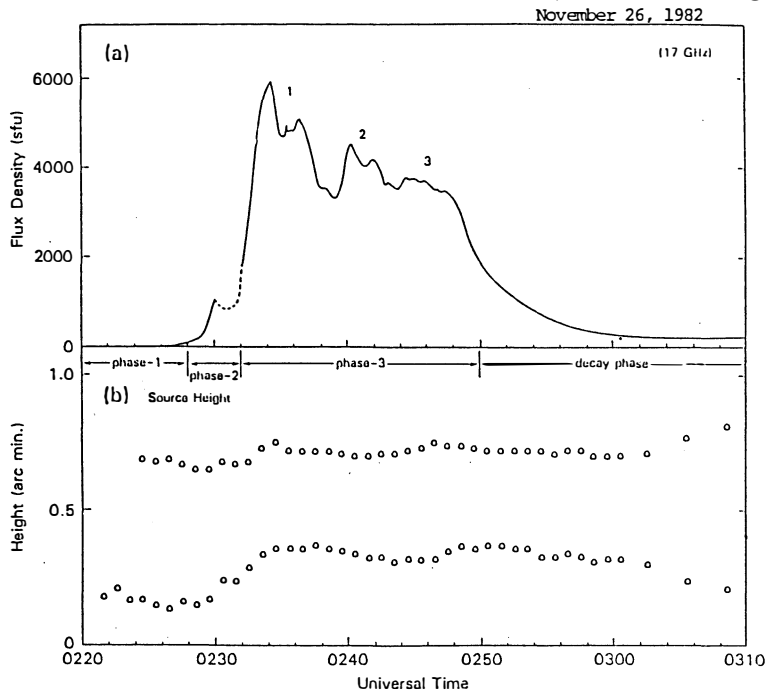

November 26, 1982

Fig. 17. (a) Time profiles of 17 GHz microwave and (b) time variation of the height of two microwave (17 GHz) sources during the 1982 November 26 Flare.

event is of much longer duration than the event on June 7, 1980, about 20 minutes compared to about 1 minute. The microwave observations were made with the 17-GHz with the hard x-ray Burst Spectrometer (HSRBS) on SMM.

(1)　The microwave burst is composed of three successive peaks with a quasi-periodicity of about 6 minutes as indicated by number 1-3 in Fig. 17(a).

(2)　Each of the microwave peaks further consists of two sub-peaks. The hard x-ray time profiles seem to coincide with the microwave sub-peaks. The SMM hard x-ray data are available only for the first peak.

(3)　The microwave and hard x-ray emissions start almost simultaneously within 10 seconds.

(4)　The microwave source is composed of two sources, one at a height of $\sim 10^4$ km and the other at $\sim 3 \times 10^4$ km. These values are derived on the acssumption that the sources are located directly above the H_α flare (S10, W88).

Figure 17(b) shows the height of the two microwave sources as a function of time. In the pre-burst phase (phase 1: 0220-0228 UT), the upper source appears at a height of $\sim 2.9 \times 10^4$ km above the photosphere and the lower one at $\sim 0.7 \times 10^4$ km. In phase 2, the lower source rises at a velocity of ~ 30 km/s. The main phase (phase 3) started when the lower source reaches a height of 1.5×10^4 km. It is suggested that the two sources collide with each other at this time. In fact, a small up-and-down motion of the lower source is observed in the main phase. The oscillation period and peak-to-peak amplitude of the up-and-down motion are $\sim$ min and $\sim 2 \times 10^3$ km (significantly larger than the fluctuation level due to the signal to noise ratio), respectively. After the main phase, the lower source begins to go down towards its previous position. On the other hand, the upper source rises gradually, though it remains at almost the same height until the decay phase.

The observational facts summarized above, especially the collision of the two microwave sources and the small up-and-down motion of the lower source in the November 26, 1982 event, suggest that the current loop coalescence takes place. The existence of two H_α bright components in the June 7, 1980 event also supported this interpretation.

3.2　Interpretation by Simulations

Two parallel current loops are unstable against the coalesceknce instability. They are attracted by and collide with each other and finally coalesce into one loop. Its nonlinear development can release a large almount of poloidal magnetic energy associated with the current loops into particle energies. We investigated this process, i.e., the global plasma dynamics, heating and acceleration of particles, and so on, through computer simulations as described in Chapter 2. Here, we made two different types of simulations in order to experiment with a a wide variety of plasma parameters: one is a MHD particle simulation, and the other a collisionless full-electromagnetic particle simulation, both of which are two-dimensional in space across the plane perpendicular to the current loops and three dimensional in velocity space.

(**a**) Explosive Coalescence --- June 7, 1980 Flare

The case where two parallel loops have sufficient electric currents that they may attract each other fast enough (in about one Alfvén transit time) was simulated using the collisionless fullelectromagnetic particle code.

The resultant time history of the electron temperature is shown in Fig. 2. We can clearly see a quasi-periodic oscillation, the period of which is about one Alfvén transit time ($8\ \omega_{c\ i}^{-1}$). The cause of this oscillation is as follows: after explosive reconnection of poloidal magnetic fields takes place at the X-point between approaching current loops, the two plasma blobs pass through each other and ovesrshoot, resulting in repetition of this process.

Fig. 2 also shows that the electron temperature oscillation is characterized by prominent double sub-peak structure. The double sub-peaks occur just before and after each peak in the magnetic field intensity. Just before a peak, the magnetic acceleration of the plasma by $J \times B$ becomes strongest so that the magnetic flux behind the colliding plasma blobs as well as the plasma blobs themselves are strongly compressed. This plasma compression causes the first sub-peak of the electron temperature. Then, the plasma particles acquire velocities close to the Alfvén velocity along the colliding direction, so that they detach from the magnetic flux against which they have deen compressed, resulting in an expansion and hence in an adiadbatic cooling of the plasma as the magnetic fields obtain peak values. After the peak in the magnetic fields, the process reverses giving rise to the second sub-peak of the electron temperature.

A similar time history is obtained for the kinetic energy of high-energy tail electrons and protons as well as for proton temperature. The acceleration of the high energy-tail particles is due to the $V_P \times B$ acceleration mechanism, which can lead simultaneous electron and proton acceleration within about second. Since these processes accompany the local plasma compression/decompression just before and after coalescence, it is not surprising that the time profile of the microwave emissions caused by high-energy tail electrons resembles that of Fig. 2 (d).

The result of this simulation can also explain the observed period of the quasi-periodic oscillation of the June 7, 1980 event. The period(~ 4 sec) which is estimated with source size (~ 5 are sec), magnetic field (~ 200 Gauss: Kiplinger et al., 1983) and emission measure ($\sim 10^{49}$ cm^{-3} from the GOES soft x-ray data).

We discuss the energy spectrum of electrons and protons, after the explosive coalescence of two current loops. The energy spectrum consists of three components; (a) background thermal component due to the adiabatic heating, (b) intermediate component due to inductive electric field, (c) high energy component due to the $V_P \times B$ acceleration. Fig. 18 shows the energy spectrum without the background thermal component which was reproduced from the previous figures given in Chapter 2.

The intermediate non-thermal component has $\gamma \cong 2$ as the power-law index near the peak, while near the valley the spectrum becomes more soft. The global structure of the electron energy spectrum is consistent with observations. (Kane et al., 1984; Kiplinger et al., 1984)

The spectrum for ions is shown in Fig. 18b in which two cases are given. The one is just after the coalescence ($T=28\ \Omega_i^{-1}$) and the other is at $T=40\ \Omega_i^{-1}$. As seen in the figure, the spectrum becomes harder which means that the number of high energy proton increases. The range (b) and (c) for protons corresponhds to the production of observed γ-rays.
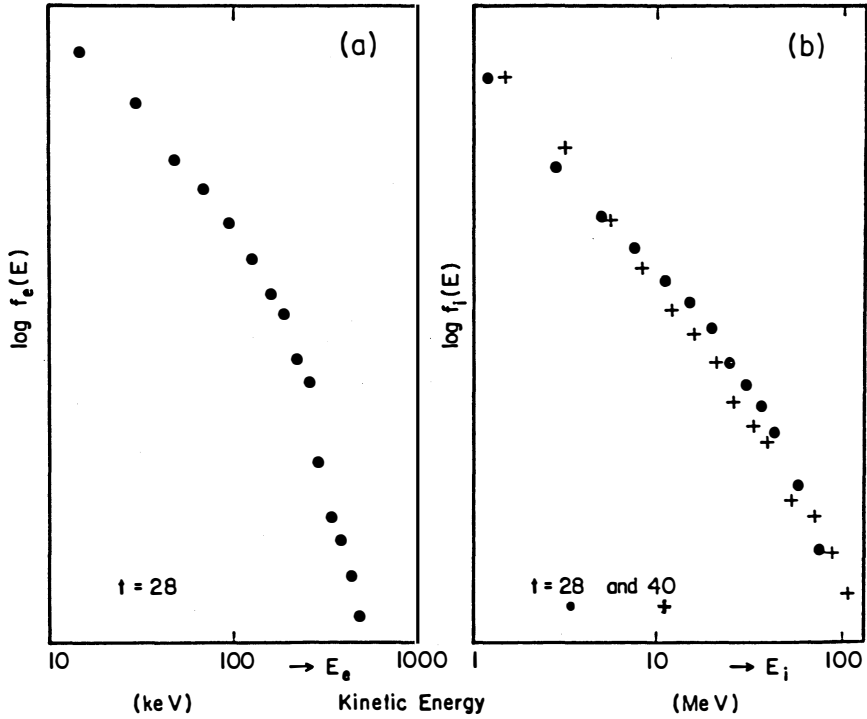
Fig. 18. (a) Electron energy spectrum just after explosive coalescence.

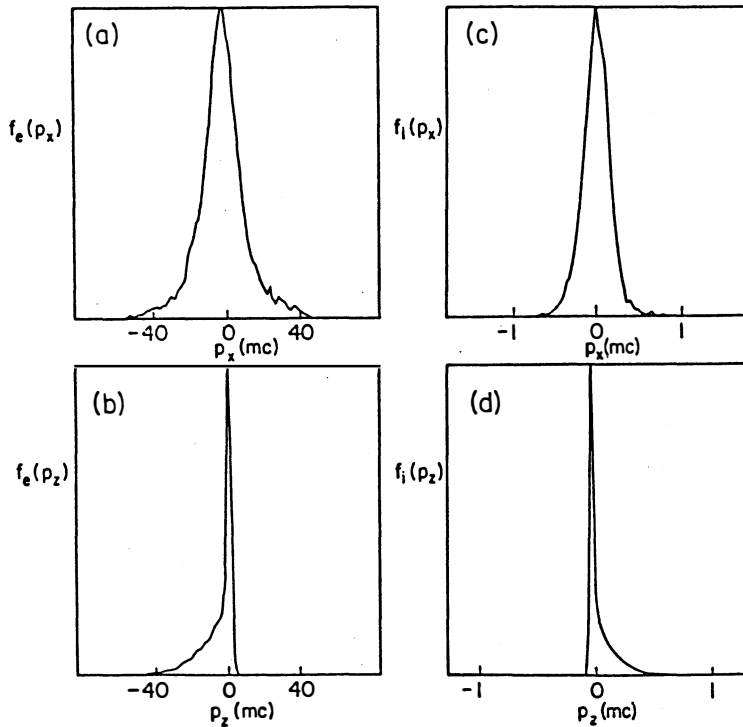(b) Proton energy spectrum just after (t=28) and later explosive coalescence (t=40).

Fig. 19. Distribution functions for electrons and protons in the case of multiple-current loop interactions.

Finally, we make brief comments about the energy spectrum in the multiple coalescence. The global behavior consisting of three energy components is still the same as the two loop coalescence (see Fig. 19). The maximum energy obtain by v_P x B acceleration depends on total released energy. Therefore the bigger flare can produce stronger γ-rays and neutrons.

(b) Slow Coalescence —— November 26 1982 Flare

When two parallel loops have insufficient electric currents or are not well separated and hence the attracting force of them is weakger than that of the previous case, reconnection of poloidal magnetic fields during loop coalescence becomes slower. (However, this reconnection rate is still faster than what would be predicted by a classical tearing theory (Furth et al., 1963)). This case was also simulated using the MHD particle code. Figrure 7 (a) shows the temporal development of plasma kinetic energy (the electron pressure energy) during the coalescence. Also shown in Fig. 7 (b) is the time history of the integrated reconnected magnetic flux through the X-point (case shown in Fig. 5(a) in Bhattacharjee, et al., 1983) Note that a slight amount of oscillations of reconnected flux can be seen around the straight line. Again we can see the oscillatory behavior with double sub-peak strucsture in both time histories, though it is less prominent compared with that of the explosive coalescence case presented in the previous subsection. The period of osciliation is about 5 times the Alfvén transit time.

The obtained time history resulting from the simulation is explained as follows. In the case of slower reconnection, the two plasma blobs do not pass through each other but are pushed back by the pressure of the magnetic field compressed between the two loops. This motion is repeated resulting in the damping oscillation shown in Fig. 7 (a). The amplitude of the oscillation in this case is less prominent compared with the previous case.

The observed plasma kinetic energy oscillation exhibit a structure quite similar to the microwave time profile of the November 26, 1982 flare as shown in Fig. 17(a). The source size of the November 26 flare is about 10 times larger than that of the June 7 flare. We therefore estimate the calculated period of the oscillation to be 5 x 4 x 10 = 200 sec, assuming that the Alfvén velocity is about the same for both cases. This period is close to the observed period of about 6 minutes. Note also that in this case the flow velocity is much below the Alfvén velocity in agreement with the observational fact that the 40 km/s colliding velocity of the lower loops is much smaller than the Alfvén velocity of $\sim 10^3$ km/s.

The results obtained from computer simulations of the coalescence instability of two current loops are in good agreement with observations of two widely differing flares. The key characteristics which are well explained are the simultaneous accelerations of both elecstrons and ions, and the double sub-peak structure in quasi-periodic pulses. The double sub-peak structure is more pronounced when the currents in the two loops are sufficient for the explosive coalescence to occur. This case corresponds to the June 7, 1980 flarce. When the currents are insufficient for the fast coalescence, the double sub-peak structure is less pronounced. This case corresponds to the November 26, 1982 flare. In addition, we have the observation suggesting the collision of the two microwave sources for the November 26, 1982 event.

4. Conclusions and Discussion

In the preceding chapters we have shown fundamental characteristics of current loop coalescence plasma dynamics and compared them with solar flare observations. The current loop coalescence has been successful in explaining several important natures of the impulsive phase as follows: (1) the sudden explosive development in time profiles, (2) simultaneous acceleration of electrons and protons up to several times their rest mass energy, (3) plasma heating due to abiabatic compression up to several times 10^7 K, and (4) quasi-periodic pulses of microwave, x-ray and γ-ray radiations and also double-peak structure in each pulse. With regard to (2), it is noteworthy that the enegy spectrum of accelerated electrons is almost consistent with observations. Further, we have revealed that the energy release due to the coalescence can be very explosive or relatively gradual depending upon various physical conditions, the key parameters of which are plasma β ratio, colliding velocity (current localization and peakness condition), and B_P / B_T. Thus this model is applicable both to very "impulsive flares" and to "gradual flares", as is shown in Chapter 3. Probably in impulsive flares such as the June 7, 1980 flare small current loops develop and interact with each other in the lower corona, while in gradual flares such as November 26, 1982 flare, large current loops whose to reaches several 10^4 km in its height, develop and interact with each other, whose current distribution might be comparable with the distance of the two loops.

So far, we have argued that the quasi-periodicity is one of the most important signatures of the two current loop coalescence, because of its ideal situation. However, the quasi-periodic pulsation is not a common phenomenon for the majority of flares. In particular, the beautiful regularity such as seen in the June 7, 1980 flare has been rarely observed. Therefore one might claim that the current loop coalescence is not a basic mechanism of solar flares, even though in some specific flares it plays a role. On the contrary, we believe that the coalescence is an elementary process commonly occurring in the impulsive phase of solar flares.

In Chapter 2 we have presented the result of a computation simulation of multiple interaction of many cnurrent filaments in addition to that of two current loop interaction. The multiple coalescence exhibits many bursts that are more irregular than the simple two current loop coalescence. In other words, it is very difficult for us to find any regularity from the resultant time profiles alone. We suggest that this is the case that happens in most flares. As is easily expected, two dominant loops with currents comparable to each other may be (rarely) hardly realized in flare-producing active regions where the photospheric magnetic configuration and the photospheric motion are very complicated.

As shown in the previous sections, the current loop coalescence model has been successful in various observed points in the impulsive energy release stage. We have shown the many characteristics of the coalescence dynamics as the element process of current interactions which might be basically of fundamental importance for the energy release process. We now discuss the preflare stage in which multiple current-filament structure as shown in Fig. 20 might be generated due to the photospheric shear motions. The H_α observations near the active
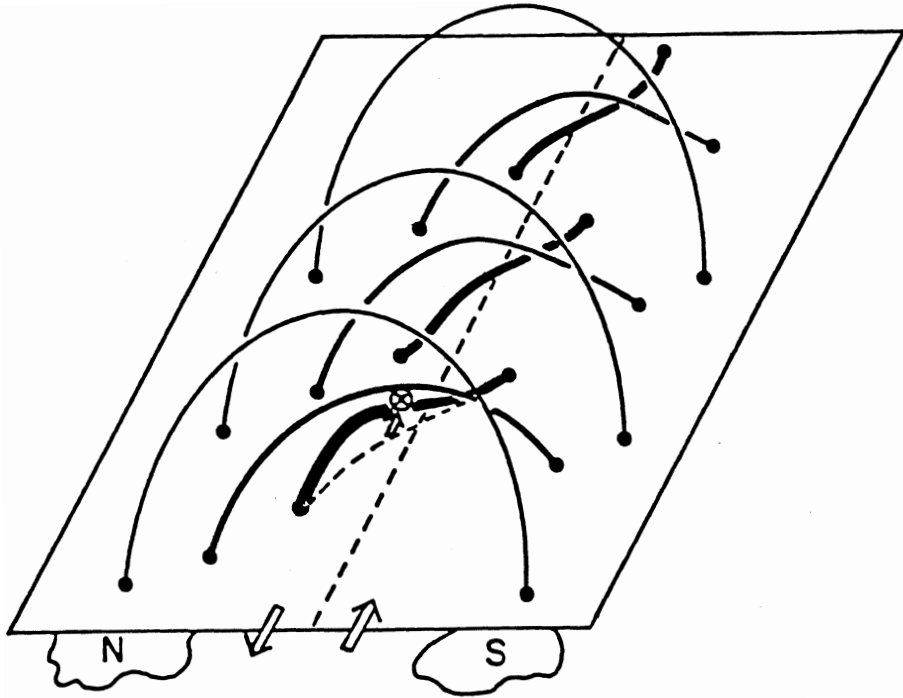
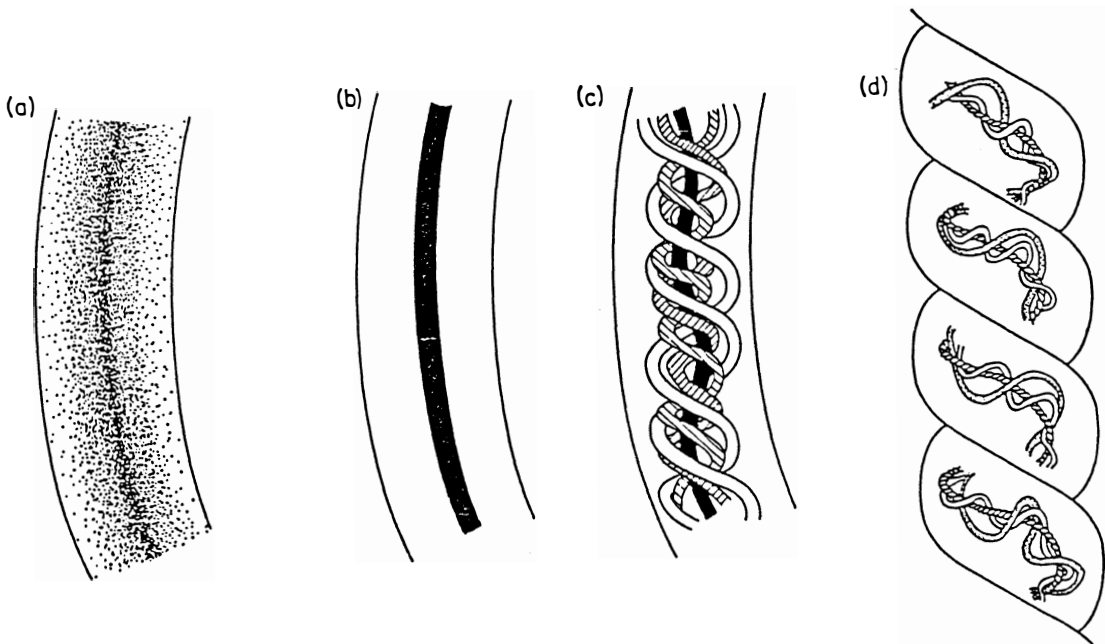Fig. 20. Multi-loop coalescence process leads to the two-ribbon flare.

(a) (b) (c) (d)

Fig. 21. Current loop generation process (a) to (d)

with line-tying effect.

region imply th it before several hours of the onset of the flare there exists photospheric shear motion across the magnetic neutral line as shown in Fig. 20. The photospheric shear motion can give rise to plasma currents along the potential magnetic field produced by the sunspots near the active region. If the photospheric motions are associated with plasma vortex motion, the current loop structure can be generated in the arcade-like structure as shown in the figure.

As the shear motions proceed, the current density can increase and the current loops might move up, associated with relaxation of magnetic tension. Recent computer simulation (Wu, 1985) suggests in the modeling of arcade-like preflare stage that the current tends to localize by its pinching effect in the low region. Recently, the preflare acceleration in the current sheet moving up across the external potential magnetic field is discussed (Sakai et al., 1986). Furthermore, the recent simulation (Aydemir et al., 1985) of current generation in the current loop with line-tying effect suggests the multi-current filament structure with different helicity as shown in Fig. 21. The multi-current filament system might ascend with increase of the current density as well as current constriction into the low region of the corona. In the low β region the current constricstion can be enhanced and each current filament can be well separated. If the current density continues to increase further, such that the·condition $B_P > B_T$ can be realized, the current loop coalescence can be set up. Of course, as seen in the multi-coalescence simulation, the poorly separated current filaments might coalesce without a large amount of energy release and can grow to high current density filaments before explosive strong energy release. A similar situation can also occur in the braized current filament system in Fig. 21.

Next we discuss the later phase after the current loop coalescence in connection with the observed two Ribbon structure. As discussed above, the flaring region might consist of multiple current loops associated with ascending motions. As shown in the figure, if the current loop coalescence happens to start locally where the condition for the explosive onset can be satisfied in the lower current loops, the sequential flaring might proceede firstly in the direction along the magnetic neutral line, as observed in the recent H_α observation (Kurokawa et al., 1985). The reason why the sequential flaring proceeds along the arcade might be due to gemometrical structure or the fact that the meta-stable filaments sit around in the same height in the corona. The flaring loops move up slowly and continue to trigger the current loop coalescence with upper currect loops. The sequential flaring on the upper loops can be observed in the H_α picture which shows slow expansion motions far from the magnetic neutral line.

We need more investigations about current filament generation in the preflare stage, in connection with the explosive current loop coalescence prpocess.

References

Aydemir, A., Tajima, T., and Sakai, J. 1985, AGU Fall Meeting, 1985.

Bai, T., Hudson, H.S., Pelling, R.M., Lin, R.P., Schwartz, R.A., and von Rosenvirge, T.T. 1983, Ap. J., 267, 433.

Bai, T., and Ramaty, R. 1979, Ap. J., 227, 1872.

Bhattachargee, A., Brunel, F., and Tajima, T. 1983, Phys. Fluids, 26, 3332.

Brunel, F., Tajima, T., and Dawson, J.M. 1982, Phys. Rev. Lett. 49, 323.

Carreras, B., Rosenbluth, M.N., and Hicks, R. 1981, Phys. Rev. Lett. 46, 1131.

Chow, Y. 1983, Private Comm nication.

de Jager, C. 1969, in COSPAR Symposium on Solar Flares and Space Science Research, ed. c. de Jager and Z. Svestka (Amsterdam : North Holland), p. 1.

Drake, J.F., and Lee, Y. C. 1977, Phys. Rev. Lett. 39, 453.

Finn, J.M. and Kaw, P. K. 1977, Phys. Fluids 20, 72.

Forrest, D.J. et. al. 1981, 17th Inter. Cosmic Ray Conf. 10, 5.

Forrest, D.J. and Chupp, E.L. 1983, Nature (Letters), 305, 291.

Furth, H.P., Killeen, J., and Rosenbluth, M.N. 1963, Phys. Fluids 6, 1054.

Gold, T., and Hoyle, F. 1960, M.N.R.A.S., 120, 89.

Heyvaerts, J,, Priest, E.R., and Rust, D. M. 1977, Ap. J., 216, 123.

Howard, R., and Svestka, Z, 1977, Solar Phys., 54, 65.

Kane, S. R., Kai, K, Kosugi, T., Enome, S., Landecker, P.B., and Mckenzie, D.L. 1983, Ap., J. 271, 376.

Kiplinger, A.L., Dennes, B.R., Frost, K.J., and Orwing, L.E. 1983, Ap. J., 273, 783.

Kurokawa, H. 1985 Private Communication.

Machado, M.E. 1985 Private Communication.

Nakajima, H., Kosugi, T., Kai, K, and Enome, S. 1983, Nature (letters) 305, 292.

Nakajima, H., Tajima, T., Brunel, F., and Sakai, J. 1984, in Proc. Course and Workshop on Plasma Astrophysics (Varenna, Italy, ESA, 1984) p. 193.

Parker, E. N. 1957, J. Geophys. Res. 62, 509.

Petschek, H. E. 1964, in Proc. AAS-NASA Symp. on Physics of Solar Flares (NASA sp-50) p. 425.

Priest, E. R. 1982, Solar Magnetohydrodynamics, (Reidel, Dordrecht).

Pritchett, P. L., and Wu, C. C. 1979, Phys. Fluids, 22, 2140.

Rutherford, P.H. 1973, Phys. Fluids, 16, 1903.

Sagdeev, R.Z., and Shapiro, V.D. 1973, JETP Lett. 17, 279.

Sakai, J., and Tajima, T. 1986, in Proec. Course and Workshop on Plasma Astrophysics (Sukhumi, USSR) Invited paper. ESA SP-251, p. 77-84.

Sakai, J., Tajima, T., and Sugihara, R. 1986, in Proc. Course and Workshop on Plasma Astrophysics (Sukhumi, USSR). ESA SP-251, p. 113-116.

Sweet, P. A. 1957, in Electromagnetic Phenomena in Cosmic Physics (Cambridge Univ. Press, London) p. 123.

Sturrock, P. A. ed. 1980, Solar Flares: Monograph from Skylab Solar Workshop II, Colorado Associated University Press.

Sugihara, R., and Midzno, Y. 1979, J. Phys. Soc. Jpn. 47, 1290.

Svestka, Z. 1976, Solar Flares (Dordrecht : Reidel)

Tajima, T., and Sakai, J. 1985, IFSR ⅩⅩ 186 and ⅩⅩ 197, Institute for Fusion Studies, University of Texas.

Tajima, T., Brunel, F., and Sakai, J. 1982, Ap. J. 245, L45.

Tajima, T., Brunel, F., Sakai, J., Vlahos, L., and Kundu, M.R. 1983, IAU Symp. No. 107. p. 197.

Tajima, T., and Sakai, J., 1986, Special Issue of the IEEE Transactions on Plasma Science on Space and

Cosmic Plasma.

Wild, J.P., Smerd, S,.F., and Weiss, A.A. 1963, Ann. Rev. Astr. Ap. 1 , 291.

Wu, S.T. 1985, Private Communication.